Research Article | Vol. 8, No. 3 | 1 Mar 2017 | BIOMEDICAL OPTICS EXPRESS 1271
Biomedical Optics EXPRESS

Heart structural remodeling in a mouse model of Duchenne cardiomyopathy revealed using optical polarization tractography [Invited]

Y. WANG,[1] K. ZHANG,[2] D. DUAN,[1,2] AND G. YAO[1,*]

[1]*Department of Bioengineering, University of Missouri, Columbia, MO 65211, USA*
[2]*Department of Molecular Microbiology & Immunology, University of Missouri, Columbia, MO 65211, USA*
[*]*yaog@missouri.edu*

Abstract: We investigated the heart structural remodeling in the mdx4cv mouse model of Duchenne cardiomyopathy using optical polarization tractography. Whole heart tractography was obtained in freshly dissected hearts from six mdx4cv mice. Six hearts from C57BL/6J mice were also imaged as the normal control. The mdx4cv hearts were significantly larger than the control hearts and had significantly higher between–subject variations in myofiber organization. While both strains showed classic cross-helical fiber organization in the left ventricle, the rate of the myocardial fiber orientation change across the heart wall was significantly altered in the right ventricle of the mdx4cv heart.

OCIS codes: (110.4500) Optical coherence tomography; (110.5405) Polarimetric imaging; (170.3880) Medical and biological imaging; (260.5430) Polarization.

References and links

1. D. Duan, "Challenges and opportunities in dystrophin-deficient cardiomyopathy gene therapy," Hum. Mol. Genet. **15**(2), R253–R261 (2006).
2. Y. J. Cheng, D. Lang, S. D. Caruthers, I. R. Efimov, J. Chen, and S. A. Wickline, "Focal but reversible diastolic sheet dysfunction reflects regional calcium mishandling in dystrophic mdx mouse hearts," Am. J. Physiol. Heart Circ. Physiol. **303**(5), H559–H568 (2012).
3. D. D. Streeter, Jr., H. M. Spotnitz, D. P. Patel, J. Ross, Jr., and E. H. Sonnenblick, "Fiber orientation in the canine left ventricle during diastole and systole," Circ. Res. **24**(3), 339–347 (1969).
4. P. A. Helm, L. Younes, M. F. Beg, D. B. Ennis, C. Leclercq, O. P. Faris, E. McVeigh, D. Kass, M. I. Miller, and R. L. Winslow, "Evidence of structural remodeling in the dyssynchronous failing heart," Circ. Res. **98**(1), 125–132 (2005).
5. D. Benoist, R. Stones, M. J. Drinkhill, A. P. Benson, Z. Yang, C. Cassan, S. H. Gilbert, D. A. Saint, O. Cazorla, D. S. Steele, O. Bernus, and E. White, "Cardiac arrhythmia mechanisms in rats with heart failure induced by pulmonary hypertension," Am. J. Physiol. Heart Circ. Physiol. **302**(11), H2381–H2395 (2012).
6. C. Mekkaoui, T. G. Reese, M. P. Jackowski, H. Bhat, and D. E. Sosnovik, "Diffusion MRI in the heart," NMR Biomed. (2015), doi:10.1002/nbm.3426.
7. F. J. Vetter, S. B. Simons, S. Mironov, C. J. Hyatt, and A. M. Pertsov, "Epicardial fiber organization in swine right ventricle and its impact on propagation," Circ. Res. **96**(2), 244–251 (2005).
8. Y. Wang and G. Yao, "Optical tractography of the mouse heart using polarization-sensitive optical coherence tomography," Biomed. Opt. Express **4**(11), 2540–2545 (2013).
9. Y. Wang, K. Zhang, N. B. Wasala, D. Duan, and G. Yao, "Optical polarization tractography revealed significant fiber disarray in skeletal muscles of a mouse model for Duchenne muscular dystrophy," Biomed. Opt. Express **6**(2), 347–352 (2015).
10. L. Azinfar, M. Ravanfar, Y. Wang, K. Zhang, D. Duan, and G. Yao, "High resolution imaging of the fibrous microstructure in bovine common carotid artery using optical polarization tractography," J. Biophoton. (2015), doi:10.1002/jbio.201500229.
11. Y. Wang, K. Zhang, N. B. Wasala, X. Yao, D. Duan, and G. Yao, "Histology validation of mapping depth-resolved cardiac fiber orientation in fresh mouse heart using optical polarization tractography," Biomed. Opt. Express **5**(8), 2843–2855 (2014).
12. C. Fan and G. Yao, "Full-range spectral domain Jones matrix optical coherence tomography using a single spectral camera," Opt. Express **20**(20), 22360–22371 (2012).
13. C. Fan and G. Yao, "Imaging myocardial fiber orientation using polarization sensitive optical coherence tomography," Biomed. Opt. Express **4**(3), 460–465 (2013).
14. Y. Wang, M. Ravanfar, K. Zhang, D. Duan, and G. Yao, "Mapping 3D fiber orientation in tissue using dual-angle optical polarization tractography," Biomed. Opt. Express **7**(10), 3855–3870 (2016).

#279545 https://doi.org/10.1364/BOE.8.001271
Journal © 2017 Received 27 Oct 2016; revised 27 Jan 2017; accepted 28 Jan 2017; published 1 Feb 2017

Biomedical Optics EXPRESS

15. B. Ciszek, D. Skubiszewska, and A. Ratajska, "The anatomy of the cardiac veins in mice," J. Anat. **211**(1), 53–63 (2007).
16. P. Agger, S. Lakshminrusimha, C. Laustsen, S. Gugino, J. R. Frandsen, M. Smerup, R. H. Anderson, V. Hjortdal, and R. H. Steinhorn, "The myocardial architecture changes in persistent pulmonary hypertension of the newborn in an ovine animal model," Pediatr. Res. **79**(4), 565–574 (2016).
17. T. A. Meyers and D. Townsend, "Early Right Ventricular Fibrosis and Reduction in Biventricular Cardiac Reserve in the Dystrophin-Deficient mdx Heart," Am. J. Physiol. Heart Circ. Physiol. **308**(4), H303–H315 (2015).
18. I. C. C. Barbin, J. A. Pereira, M. Bersan Rovere, D. de Oliveira Moreira, M. J. Marques, and H. Santo Neto, "Diaphragm degeneration and cardiac structure in mdx mouse: potential clinical implications for Duchenne muscular dystrophy," J. Anat. **228**(5), 784–791 (2016).
19. D. J. Stuckey, C. A. Carr, P. Camelliti, D. J. Tyler, K. E. Davies, and K. Clarke, "In vivo MRI characterization of progressive cardiac dysfunction in the mdx mouse model of muscular dystrophy," PLoS One **7**(1), e28569 (2012).

1. Introduction

Duchenne cardiomyopathy describes the dilated cardiomyopathy seen in later-stage Duchenne muscular dystrophy (DMD) patients. It is a leading cause of morbidity and mortality in DMD patients [1]. The mdx4cv mouse is one of the most commonly used DMD animal models where the dystrophin expression is blocked by a point mutation [1]. Mdx4cv mice develop a progressive cardiomyopathy that shares many features with the human disease [1]. Although mdx4cv mice have been studied extensively, the heart structural remodeling in this model has not been investigated in detail [2]. The heart is a highly adaptive organ and its structure may change in response to progressive deterioration of cardiac function. It is known that the myofibers in a healthy heart are organized in an exquisite and optimized structure [3], which was often altered in heart diseases as part of the pathological remodeling process [4, 5]. The knowledge of detailed myocardial fiber changes during disease progression is essential for understanding the intricate structure-function relationship in heart diseases.

The MRI based diffusion-tensor imaging (DTI) technology is the only practically available tool for imaging myocardial fiber structure in the whole heart [6]. However, in addition to its high system cost, the limited spatial resolution of DTI makes it extremely challenging for revealing detailed myocardial fiber structure in the small mouse hearts. A typical mouse heart has a diameter of ~6 mm with 1~2 mm thick ventricular wall and the myofiber orientation can change over 100° across the thin ventricular wall [6, 7]. Abrupt orientation changes of more than 50° were observed between different epicardial layers [7]. Therefore, a sufficient resolution is important for correctly imaging detailed fiber orientation changes in the ventricular wall of the heart.

Optical polarization tractography (OPT) is a newly developed method that can image high-resolution fiber organization in fibrous tissues [8–10]. It was based on the Jones matrix implementation of the polarization-sensitive optical coherence tomography (PSOCT). OPT uses Jones calculus to construct the depth resolved optic axis for measuring fiber orientation with microscopic resolution [11]. In this study, OPT was applied to image the myocardial fiber structures in freshly excised whole mouse hearts. The results revealed significant structural remodeling in the mdx4cv mouse model of Duchenne cardiomyopathy.

2. Methods

2.1 OPT system

The OPT method was implemented in a 0.85 μm wavelength spectral-domain Jones matrix PSOCT system which has been described in detail previously [12, 13]. Briefly, the system measures pixel-wise Jones matrix of the sample by using incident light with alternating right- and left-circular polarizations. For each incident polarization, the horizontally and vertically polarized components of the interference signals were detected using a custom spectrometer equipped with a 1024-pixel line scan camera running at 50k A-lines/sec. An iterative Jones calculus based algorithm was applied to extract the depth-resolved optic axis for mapping the

Biomedical Optics EXPRESS

fiber orientation [13]. The fiber orientation measured is between [-90°, 90°] and represents the projected orientations within the plane perpendicular to the incident light [8, 14], which is analog to the "helix" angle measured in DTI [2, 7]. The system has a 12.4 μm lateral resolution at the focus and a 5.9 μm axial resolution in tissue.

2.2 OPT imaging of a whole mouse heart

All animal experiments were approved by the institutional animal care and use committee. The freshly excised hearts from six 7-mo old male B6Ros.Cg-DMD$^{mdx\text{-}4cv}$/J mice (the "mdx" group) and six age-matched male C57BL/6J mice (the "BL6" group) were imaged using the OPT system. The procedure to image the whole heart tractography was described in details previously [8]. Briefly, the heart was mounted on a rotational stage via a 20-gauge needle passing through the long axis of the heart (between the apex and center of the base). The needle was fixed on the base of the stage and was aligned with the rotational axis. During imaging, the stage was rotated continuously over 360° at a speed of 1.25°/s while the light repeatedly scanned along the long axis of the heart (as the B-scan) using a galvanometer coupled with a telecentric lens (36 mm focal length). Each B-scan covered 8 mm with 2000 A-scans. A total of 3600 B-scans were acquired at a speed of 12.5 B-scans/s and took 288 s. The heart diameter was measured using a caliper.

The constructed 3D data set of fiber orientation had 280 × 2000 × 3600 pixels (in A × B × C scans) and covered a corresponding imaging area of 1.1mm × 8.0mm × 360°. The 2D "planar" tractography was first built at each *en face*s plane using Matlab streamline functions [8]. A 5 × 5 (pixels) median filter was applied to all processed B-scan images to improve signal-to-noise. The stack of the "planar" 2D tractography was then polar-transformed into the 3D coordinates from the measured heart diameter and heart surface [8]. The OPT results were visualized using the 3DSlicer software (www.slicer.org).

3. Results and discussion

Figure 1(a) shows intensity images of a BL6 and an mdx mouse heart. The BL6 heart appeared in a pear-like shape; whereas the mdx heart was bigger and close to a cylindrical shape. In all hearts tested, the mdx heart had an average diameter of 6.88 ± 0.48mm which was significantly larger (p = 0.013, Student's t-test) than the BL6 heart (6.15 ± 0.25 mm).

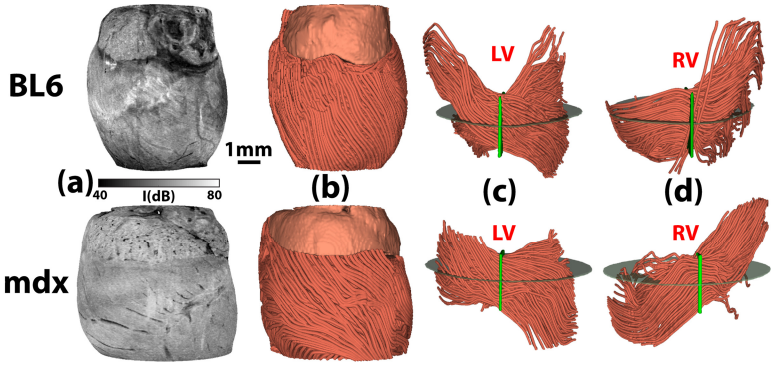

Fig. 1. (a) Intensity images of a BL6 heart (Visualization 1) and an mdx heart (Visualization 2). (b) The corresponding 3D tractography of the BL6 heart (Visualization 3) and the mdx heart (Visualization 4), both with the left ventricle (LV) facing front. Also shown are depth-resolved tractography showing myofibers passing through a 1.5 mm high region of interest (green plate) across (c) the LV (Visualization 5 and Visualization 6) and (d) the right ventricle (RV) (Visualization 7 and Visualization 8) of the BL10 and mdx hearts, respectively.

Figure 1(b) illustrates the global ventricular tractography of the same two hearts shown in Fig. 1(a). Since no clear optic axis data was obtained in the atrial and aorta tissues, they were shown in solid color. The fiber tractography shown in Fig. 1(b) was obtained at the 100 μm

Biomedical Optics EXPRESS

depth beneath the epicardium. The associated animations revealed the change of the fiber orientation of the entire heart. Overall, the fiber orientation appeared similar in the left ventricle (LV) of both the BL6 and mdx hearts, but quite different in the right ventricle (RV). To examine depth-resolved fiber orientation across the ventricular wall, Figs. 1(c) and 1(d) showed myocardial fibers that pass through a 1.5 mm high (along the B-scan) region of interest (ROI) located at the center of the LV and RV, respectively. The associated animations show the change of myofiber structure from the epicardium to the endocardium.

In both strains, the LV showed the classic "cross-helical" profile [3] (Fig. 1(c)). "Negatively orientated" fibers at the epicardium transitioned to circumferential at the middle of the ventricular wall, and became positively oriented toward the endocardium. However, the mdx heart appeared to have smaller helix angles and a smaller rate of orientation change over the LV wall than the BL6 heart. The myofibers in the BL6 RV had much less orientation changes across the heart wall than in the LV. The BL6 heart showed some "vertical" fibers close to the RV surface at the proximity of the right ventricle vein (RCV) [15]. This was not observed in the mdx heart. The RV of the mdx heart appeared to have more variations in fiber organization in the *en face* plane than the BL6 heart.

We further quantitatively analyzed the depth-resolved fiber organization in the hearts. To compensate for the variation in heart structure among different hearts, an evaluation "window" was defined in both the LV and RV based on common structural features including cardiac veins [15] observed in the intensity images of the mouse hearts (Fig. 2(a)). The vertical yellow dashed line was first drawn along the B-scan direction from the lowest boundary of the left atrium. This line ended at the intersection with the left cardiac vein (LCV) [15]. The middle point of this line was then identified as the center of the LV window ("Lc" in Fig. 2(a)). In addition, the white dashed line was drawn across the Lc along the C-scan direction. The intersection of this line with the RCV was selected as the center of the RV window ("Rc" in Fig. 2(a)). The two evaluation windows were then created by extending from their corresponding centers to reach a size of 2.8 mm × 70° (700 × 700 pixels, B × C) as illustrated as the blue boxes in Fig. 2(a). These windows were manually determined in all hearts and their coordinates were recorded for subsequent calculations.

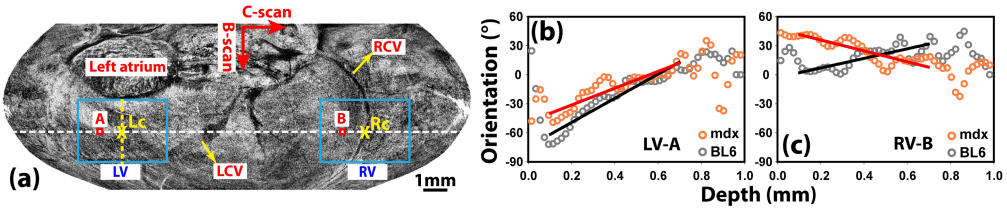

Fig. 2. (a) An illustration of the "window" in LV and RV (blue boxes) for quantitative analysis. LCV: left cardiac vein; RCV: right cardiac vein [15]. Also shown are example depth profiles of myocardial fiber orientation calculated at ROIs in the (b) LV and (c) RV as labeled in red boxes in (a). These sample data were obtained from the same hearts shown in Fig. 1.

Figures 2(b) and 2(c) show depth profiles of the fiber orientation at representative region-of-interests (ROIs) inside the LV and RV, respectively. The ROIs were marked as red boxes on the white dashed line in Fig. 2(a). The ROI size was 0.1 mm × 2.5° (25 × 25 pixels in B × C). The fiber orientation values were obtained using circular averaging within the ROI [10]. Consistent with the global tractography in Fig. 1, the depth-profiles of the fiber orientation in the LV showed the "cross-helical" transition from negative to positive orientation in both the BL6 and mdx hearts. An "inversed" transition (from positive to negative orientations) was observed in the BL6 heart within 100 μm from the epicardium; but this was not clear in the mdx heart (Fig. 2(b)). Such an inverse trend was also observed in our previous studies [11] and reported in a recent high resolution (9.4-T) DTI study of the larger ovine heart [16]. This was not reported in DTI studies of healthy mouse hearts [6], likely due to insufficient resolution. The fiber orientation of the BL6 RV was slightly positive with small changes

Biomedical Optics EXPRESS

across the ventricular wall. However, the mdx heart showed a significant "negative" trend of orientation changes over the depth.

Linear fitting was applied to calculate the "slope" of the orientation change between 0.1 and 0.7 mm in depth. Orientation data within the 0.1 mm from the heart surface were excluded in the fitting to avoid the "inverse" trend shown in Fig. 2(b). The fitted slopes were 124.9°/mm (R^2 = 0.91 and root-mean-square-error (RMSE) = 7.0°) in the BL6 LV and 86.8°/mm (R^2 = 0.81 and RMSE = 7.4°) in the mdx LV. For the RV curves (Fig. 2(c)), the obtained slopes were 49.5°/mm (R^2 = 0.61 and RMSE = 6.8°) in the BL6 heart and −56.5°/mm (R^2 = 0.70 and RMSE = 6.5°) in the mdx heart.

The "slope" of the fiber orientation change with depth was calculated for all the ROIs of the same size (0.1 mm × 2.5°) within the entire LV and RV evaluation windows. In other words, the depth profiles similar to those shown in Figs. 2(b) and 2(c) were constructed and linearly fitted for a total of 28 × 28 = 784 ROIs inside the evaluation window. The slope values can be color-coded for visualization (Fig. 3(a)). The image width of the mdx heart was wider along the C-scan direction because the mdx heart had a bigger diameter. More than 92.9% of the LV regions in both hearts had fitting R^2>0.6 or RMSE<10°. The slopes were relatively homogeneous in the LV of both the mdx and BL6 hearts; but the values were overall smaller in the mdx heart than the BL6 heart. The depth profiles in the RV showed more location-dependent variations in both hearts. However, the variations in the mdx heart were bigger. Only 68.8% of the mdx RV and 84.9% of the BL6 RV had fitting R^2>0.6 or RMSE<10°. Poorer linear fitting in the RV was also reported in previous DTI studies [5]. The fitting in the RV was also affected by the presence of the RCV as more abrupt orientation changes were observed at the proximity of the RCV.

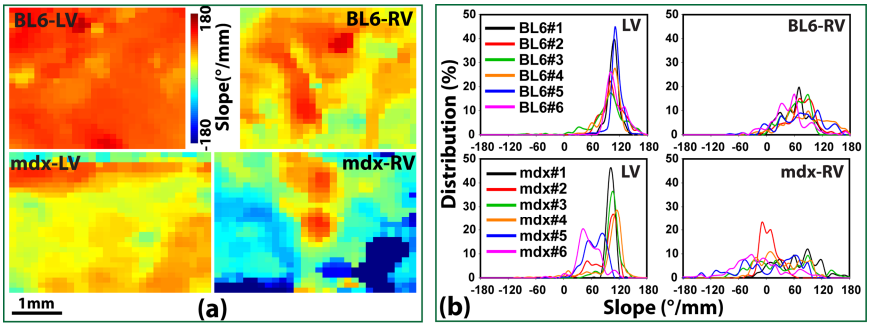

Fig. 3. (a) Examples of color-coded "slopes" of fiber orientation change with depth in the LV and RV of the same hearts shown in Fig. 2. (b) Distributions of the fiber orientation slopes obtained in all six BL6 hearts and six mdx hearts within the same LV and RV evaluation windows as defined in Fig. 2(a). BL6#1 and mdx#6 were the mice used in (a).

Figure 3(b) shows the distributions of the orientation slopes obtained in all experimental animals. The regions with fitting R^2<0.6 and RMSE>10° were not used in the calculation. Overall, the linear fitting in the mdx heart had R^2 = 0.81 ± 0.05 and RMSE = 8.19° ± 1.54° in the LV, and R^2 = 0.64 ± 0.10 and RMSE = 8.99° ± 1.28° in the RV. These fitting performance was similar to those of the BL6 heart: R^2 = 0.82 ± 0.03 and RMSE = 8.25° ± 0.47° in the LV, and R^2 = 0.68 ± 0.08 and RMSE = 8.51° ± 1.91° in the RV. The distributions in the BL6 LV were highly consistent and the rate of orientation change was 100 ~110°/mm at the peak position of the distribution. The distribution in the mdx LV varied among six mice with three hearts showing similar distributions as that of the BL6 heart; whereas the other three had broader distributions and a shift toward smaller slope values. Although the distributions in the RV were generally broader than that in the LV, the BL6 hearts still showed quite consistent distributions with positive slope values in more than 96.2% of the RV regions. However, all mdx RV curves showed much broader distributions with 38.8% of the mdx RV had negative slope values (−38.3 ± 34.0°/mm in average).

Biomedical Optics EXPRESS

Figure 4 shows the group comparison of the mean slope of the orientation change over depth obtained in all hearts. All the hearts showed "positive" slopes in the LV. The mdx group had smaller slope values (86.4°/mm ± 20.4°/mm) than the BL6 group (104.4°/mm ± 7.0°/mm) in the LV; but the difference did not reach statistical significance (p = 0.085, Student's t-test). However, the Levene's test indicated that the mdx group had a bigger variance in the slope data of the LV (p = 0.018). The group difference was more drastic in the RV where the variance was similar in both groups (p = 0.075, Levene's test). The group average of the slope was significantly smaller (p = 0.004, Student's t-test) in the mdx RV (20.3 ± 28.4°/mm) than in the BL6 RV (67.9 ± 12.6°/mm).

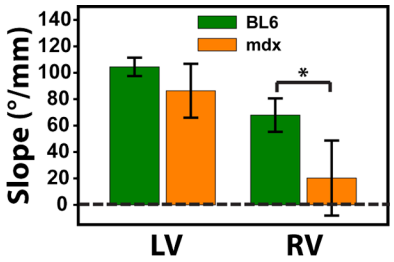

Fig. 4. A group comparison of the average rate of fiber orientation change with depth in the LV and RV of the six BL6 mice and six mdx mice. * p<0.01.

The severe structural remodeling observed in the RV of the 7-month-old mdx mouse is most likely caused by the diaphragm degeneration related pulmonary dysfunction [17, 18]. Deterioration of the respiratory function increases pulmonary vascular resistance which then leads to increased RV stress [17]. This process eventually results in tissue damage in the RV [17, 18]. The global heart structural remodeling can be a direct consequence of the myofiber damage in the RV. The large between-animal variations of the fiber organization observed in the LV of the mdx model may be indications of different disease progression in individual mice. More systematic studies are warranted to clarify the pathological process leading from local cardiac muscle damage to changes in the global heart structure.

The ~1.0 mm imaging depth achieved in this study was mainly limited by the 0.85 μm light source. The ventricular wall thickness of the 7-mo mouse heart is ~1.0 mm [19] and the RV wall is thinner than the LV wall. The 1.0 mm depth may not be sufficient to image through the entire LV wall. The imaging depth in heart can be improved by using a longer wavelength (e.g. 1.3 μm). The mdx hearts have similar ventricular wall thicknesses as the controls before 9-month of age [19]. Therefore the significantly different slope in fiber orientation changes over the depth cannot be caused by any differences in the wall thickness. It is important to note that this study only measured the helix angle of the 3D myocardial fiber located within the plane perpendicular to the incident light [2, 8]. Therefore, any orientation changes in planes that are parallel to the incident light were not detected. Imaging the true 3D fiber orientation is necessary to fully characterize the fiber structure changes, which can be realized using a variable-incident angle implementation of the OPT [14].

5. Conclusions

The OPT technology was applied to investigate the structural remodeling in the hearts of the mdx4cv mouse model of the Duchenne cardiomyopathy. OPT revealed significantly altered myocardial fiber organization in the hearts of 7-mo old mdx4cv mice in particular in the RV. This study demonstrated the potential of OPT as a useful imaging technique for studying high-resolution heart structural remodeling in small animal models of heart diseases.

Funding

This work was supported in part by the University of Missouri System Research Board and Department of Defense (MD150133).